

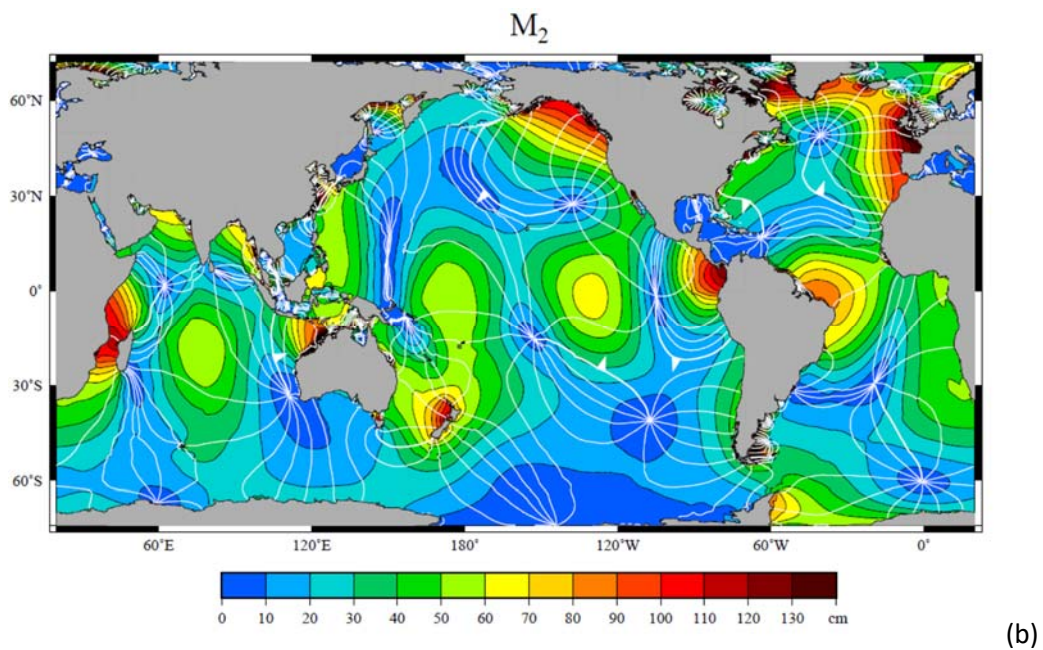
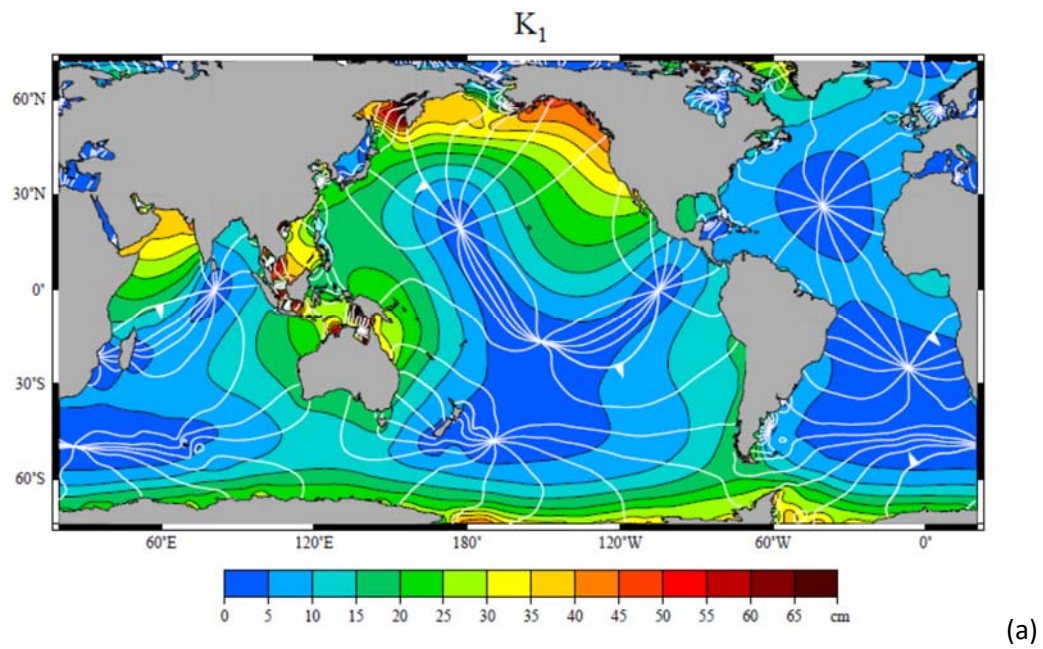
## Supplementary Material

### Supplementary Data Set

The ASCII file 'M1prime\_and\_M1\_values' contains a line for each of the 794 records from the GESLA-2 data set employed in this study. Each line shows longitude (east), latitude, amplitude ( $H_2$ , mm) and Greenwich phase lag ( $G_2$ , deg) of  $M1'$ , amplitude ( $H_3$ , mm) and Greenwich phase lag ( $G_3$ , deg) of  $M1$ , and the file name in the data set. In each case, the amplitudes and phase lags were obtained from an optimal solution of Equation 2 by sampling amplitudes in increments of 0.2 mm and phases in increments of  $2^\circ$ .

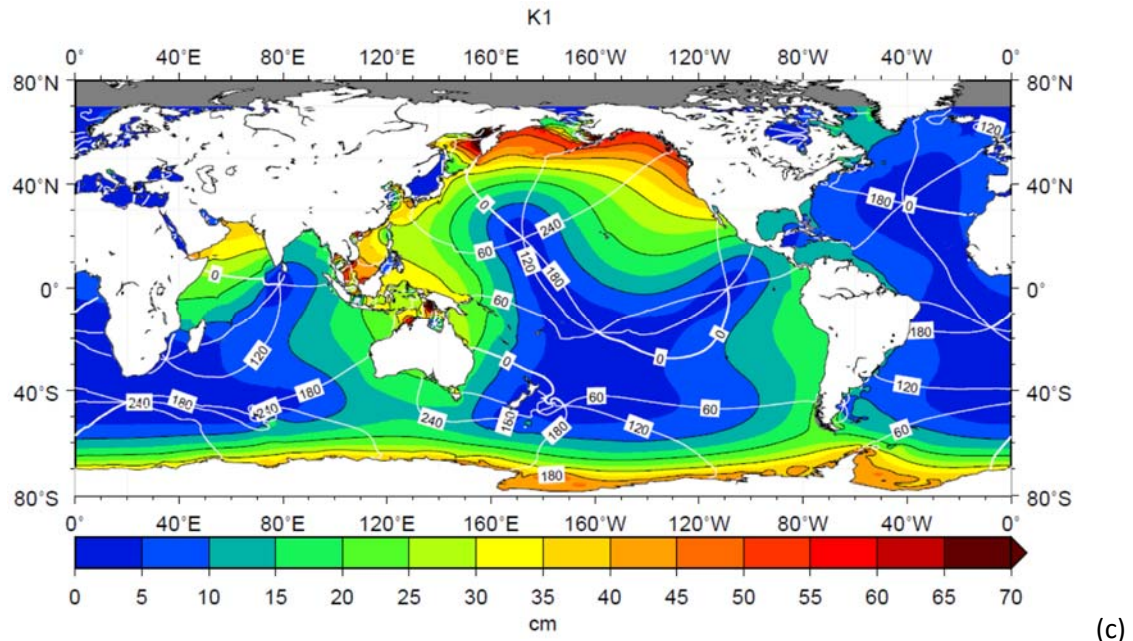
The 794 records contain 258 for which there is more than one record from the same location (defined by the stated longitudes and latitudes in a record being within  $0.05^\circ$  of those in another record). These alternative records arise from tide gauge data being contributed to GESLA-2 from more than one centre (see Table 2 of Woodworth et al., 2017). However, the alternative records do not necessarily contain the same years of information, and so it seemed reasonable to include all of them in the analysis, provided that the requirement was met for at least 9 near-complete years of data in a record as described in Section 3.

The alternative records provide a check on the derived amplitudes and phases, the magnitude of the vector-difference between alternative  $M1'$  or  $M1$  values being in almost all cases less than 1 mm.

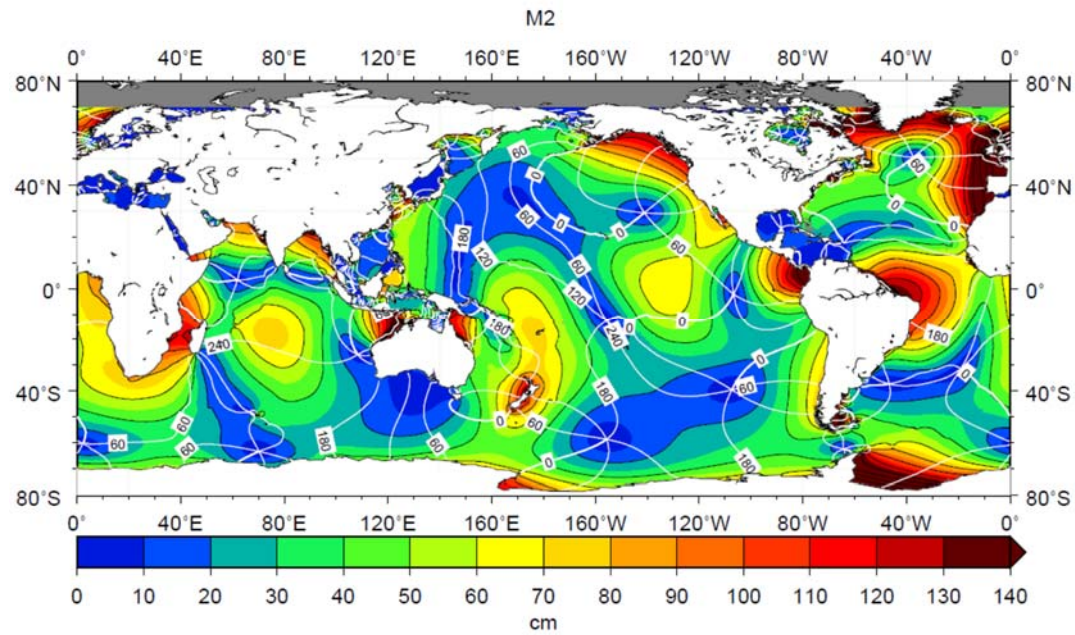


Supplementary Figure 1.

(a,b) Co-tidal charts of the K<sub>1</sub> and M<sub>2</sub> ocean tides based on satellite altimeter data provided by Dr. Richard Ray (Goddard Space Flight Center). The lines indicate Greenwich phase lag every 30°, a lag of zero degrees being shown by the bold line, and the arrows showing the direction of propagation. The colours show amplitudes. From Pugh and Woodward (2014).



(c)



(d)

(c,d) Co-tidal charts of the K1 and M2 ocean tides from the global tide model used for this study. The lines indicate Greenwich phase lag every 60°, a lag of zero degrees being shown by the bold lines. The colours show amplitudes.

The model is a global version of the regional tide-surge model of Roger Flather (e.g. Flather, 1988). An earlier version with 1-degree bathymetry had been used in studies of the ocean response to air pressure changes (Mathers and Woodworth, 2001). The present version uses a ¼-degree bathymetry derived from the General Bathymetric Chart of the Oceans (GEBCO) (Weatherall et al., 2015), together with the sub-gridscale parameterisation of Mathers and Woodworth (2001), and with an open boundary at 70°N. The model is driven only by the tidal potential of selected constituents. A degree-2 diminishing factor of 0.69 was used, except for a special value of 0.74 for K1 to allow for the ‘nearly

diurnal free wobble' (NDFW) of the rotating fluid core, and a degree-3 diminishing factor of 0.80 (Wahr, 1991).

As a rigorous parameterisation of self-attraction and loading would have been computationally expensive (and difficult to implement in the present code), use was made of the classic 8.5% scaling factor of Accad and Pekeris (1978); alternative simple schemes discussed by Ray (1998) and Stepanov and Hughes (2004) were investigated but did not result in significant improvement. As is well known, models such as this result in unfeasibly large tidal amplitudes unless energy can be dissipated by some means, which in the real ocean happens via the generation of internal tides (Ray and Egbert, 2017). In the present case, horizontal eddy viscosity is employed in order to have a more 'glue-like' ocean. Runs were made spanning 19 days, of which 5 days were spin-up from a cold start, and 14 days provided hourly values for harmonic analysis.

In spite of the model deficiencies, an optimum choice of parameters provides charts for M2 and K1 that have many similarities to those obtained from the most recent models. The colour scales in (c,d) have been chosen to be similar to those in (a,b). A comparison for K1 in (c) to that in (a) shows a similar set of amphidromic rotation centres, although slightly displaced from their real positions as expected from the inadequate loading treatment. Amplitudes are similar in the North Pacific, NW Indian Ocean and South China Sea, but larger than in (a) to the north of Australia, on the Pacific coast of South America and around Antarctica.

A comparison for M2 in (d) to that in (b) shows comparable amplitudes in the North Atlantic, North Pacific and western Indian Ocean, but larger values off the west coasts of South America and Africa, north of New Zealand, in the central Indian Ocean and in the Weddell Sea; the latter may be partly due to inadequacies in the bathymetry under the ice shelf. Most amphidromic centres are represented adequately, together with the pattern of co-tidal lines, with the exception of the SE Pacific where there are significant phase differences, presumably owing to the inadequate loading and relative lack of bathymetric information in this part of the ocean. Phase lags are even largely correct in the North Atlantic where one might have expected them to be imprecise owing to the open boundary. Although M2 amplitudes can be reduced to more realistic levels by adjusting the model parameters, it proved difficult to do that without affecting the pattern of co-tidal lines for both M2 and K1. Overall, the choice of parameters is a compromise.

However, the aim of this exercise was not to provide a model that was as good as the recent ones discussed by Stammer et al. (2014), but simply to provide one that was realistic in most respects, and that could be used as a research tool to investigate M1. Further modelling of M1 using better tide models is to be welcomed. There are several which provide a more correct representation of the physics of the barotropic and internal ocean tide without requiring the assimilation of altimeter data (e.g. Arbic et al., 2010).

#### Additional References

Accad, Y. and Pekeris, C.L.: Solution of the tidal equations for the  $M_2$  and  $S_2$  tides in the world oceans from a knowledge of the tidal potential alone, *Philos. T. R. Soc. Lond., A*, 290, 235-266, doi:10.1098/rsta.1978.0083, 1978.

Arbic, B.K., Wallcraft, A.J., and Metzger, E.J.: Concurrent simulation of the eddying general circulation and tides in a global ocean model, *Ocean Model.*, 32, 175-187, doi:10.1016/j.ocemod.2010.01.007, 2010.

Mathers, E.L., and Woodworth, P.L.: Departures from the local inverse barometer model observed in altimeter and tide gauge data and in a global barotropic numerical model, *J. Geophys. Res.*, 106, C4, 6957-6972, doi:10.1029/2000JC000241, 2001.

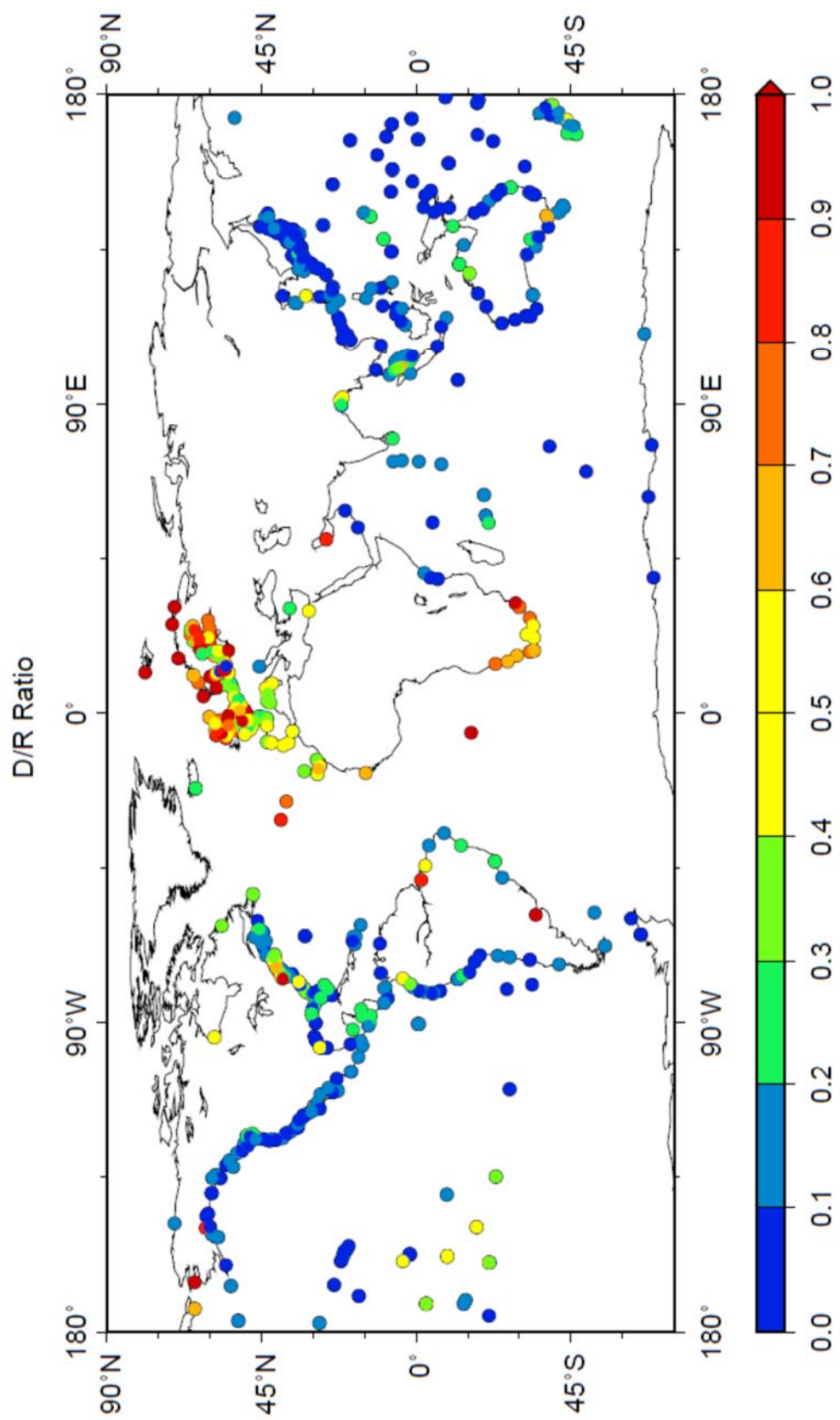
Ray, R.D.: Ocean self-attraction and loading in numerical tidal models, *Mar. Geod.*, 21, 181-192, doi:10.1080/01490419809388134, 1998.

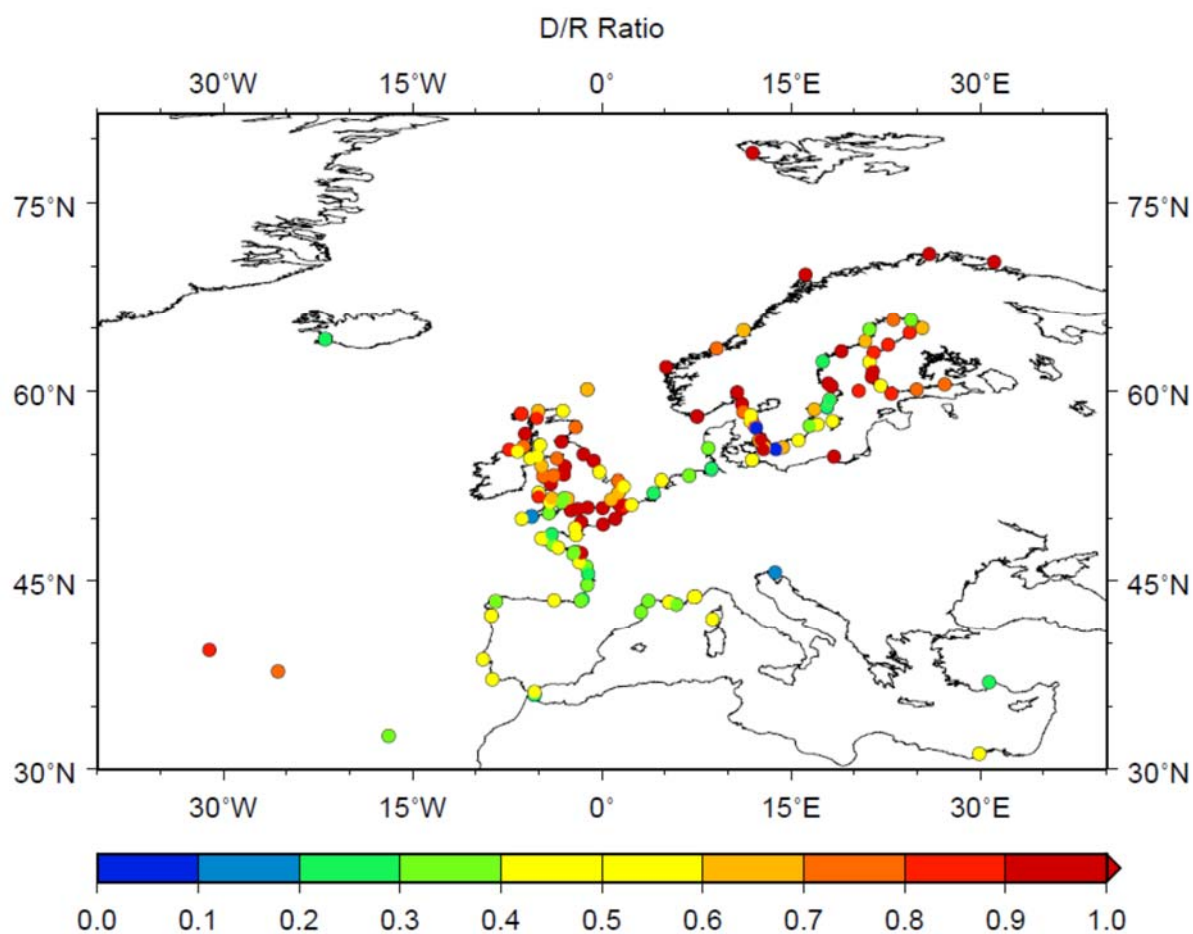
Ray, R.D., and Egbert, G.D.: Tides and satellite altimetry, Chapter 13 (p.427-458) in, *Satellite altimetry over oceans and land surfaces* (eds. D. Stammer & A. Cazenave), Boca Raton: CRC Taylor and Francis, 670pp, 2017.

Stepanov, V.N., Hughes, C.W.: Parameterization of ocean self-attraction and loading in numerical models of the ocean circulation, *J. Geophys. Res.*, 109, C03037, doi:10.1029/2003JC002034, 2004.



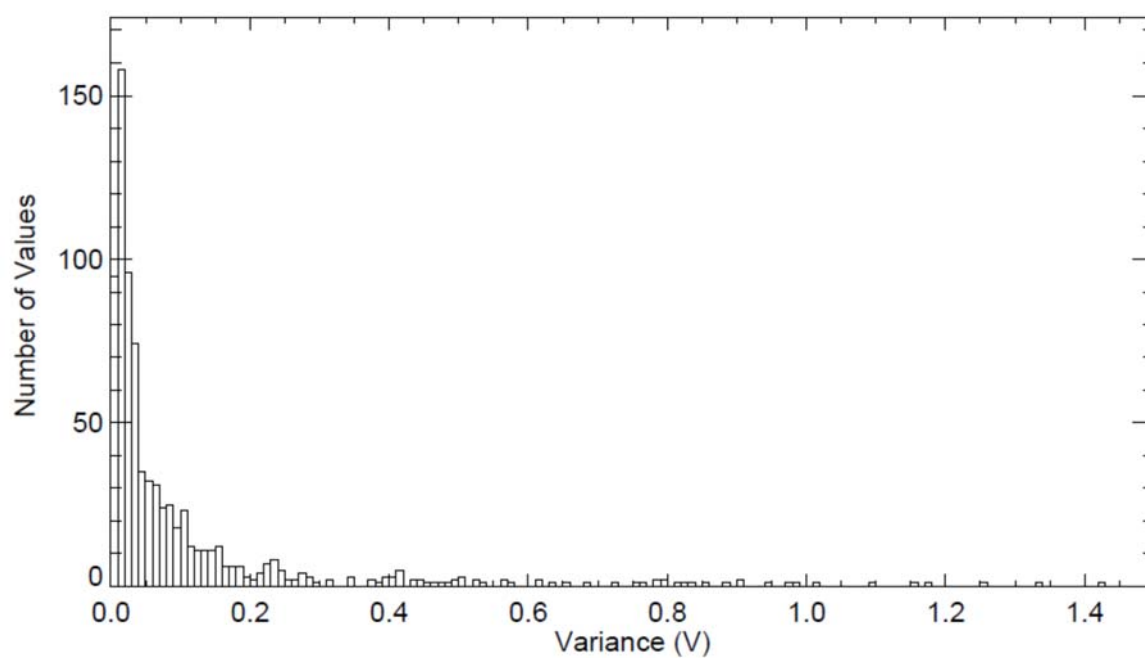
(a)



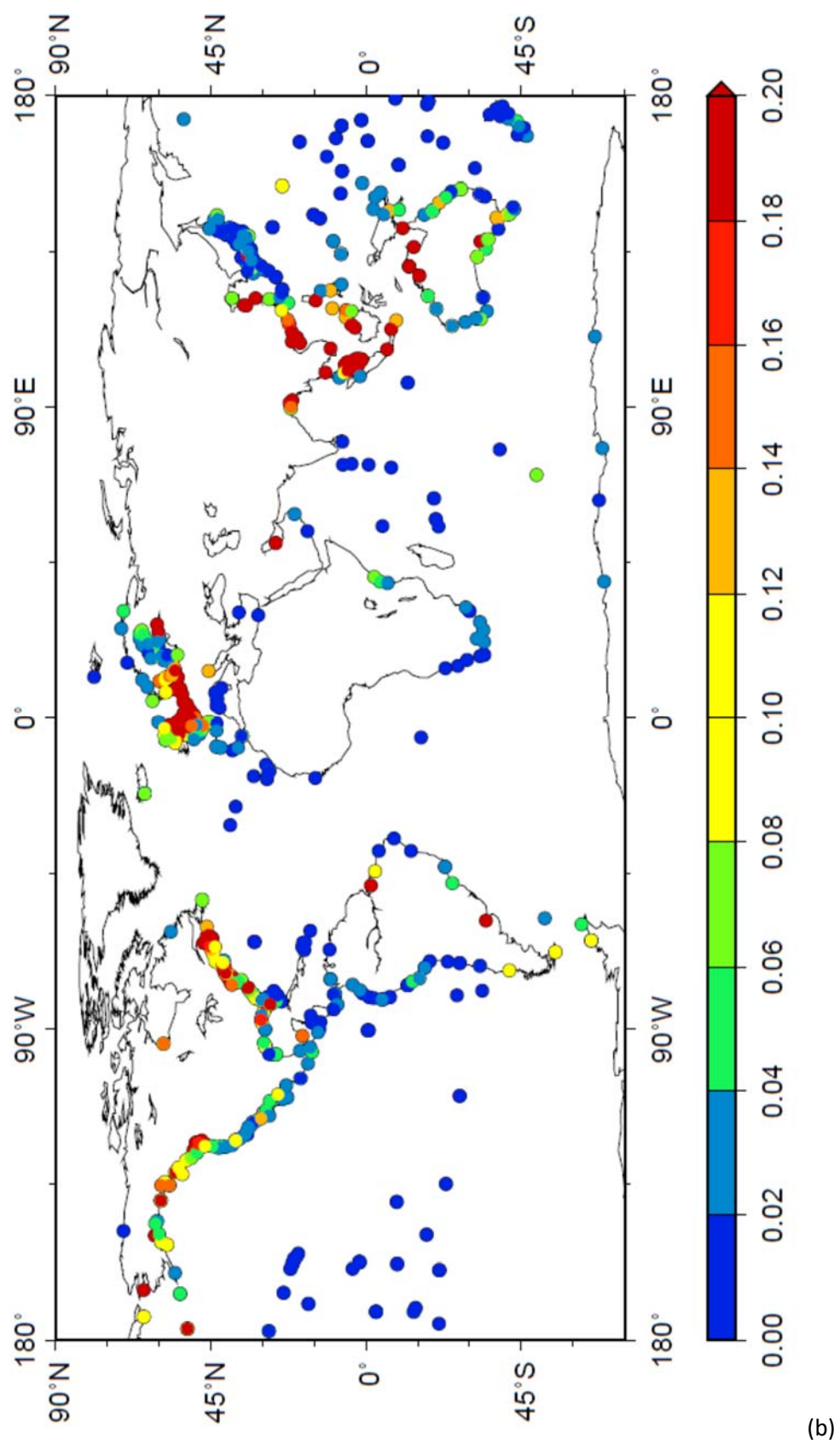


(b)

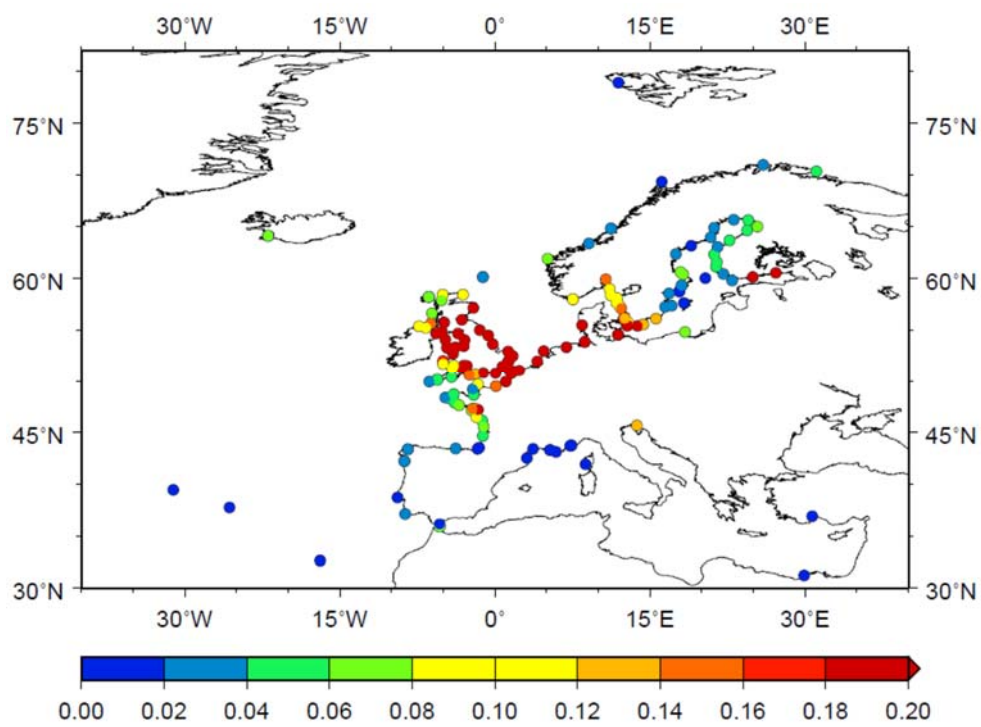
Supplementary Figure 2. Ratio D/R calculated for M1' as described in the text for (a) worldwide and (b) NW Europe.



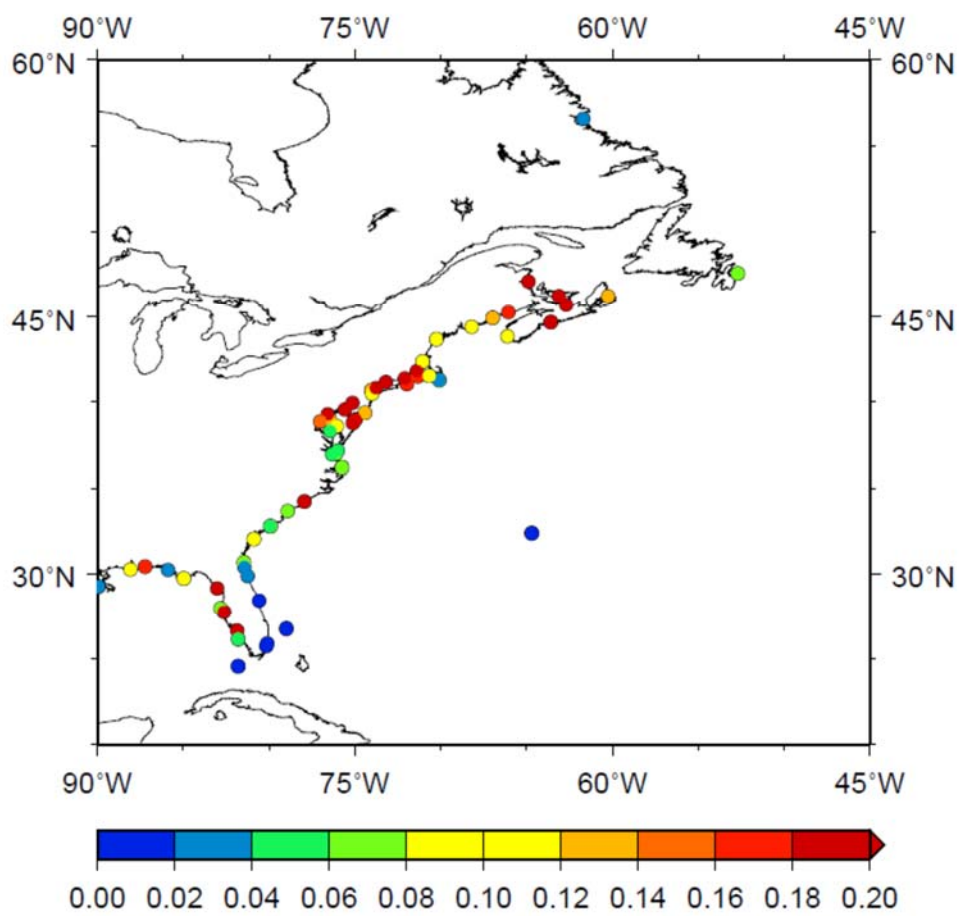
(a)



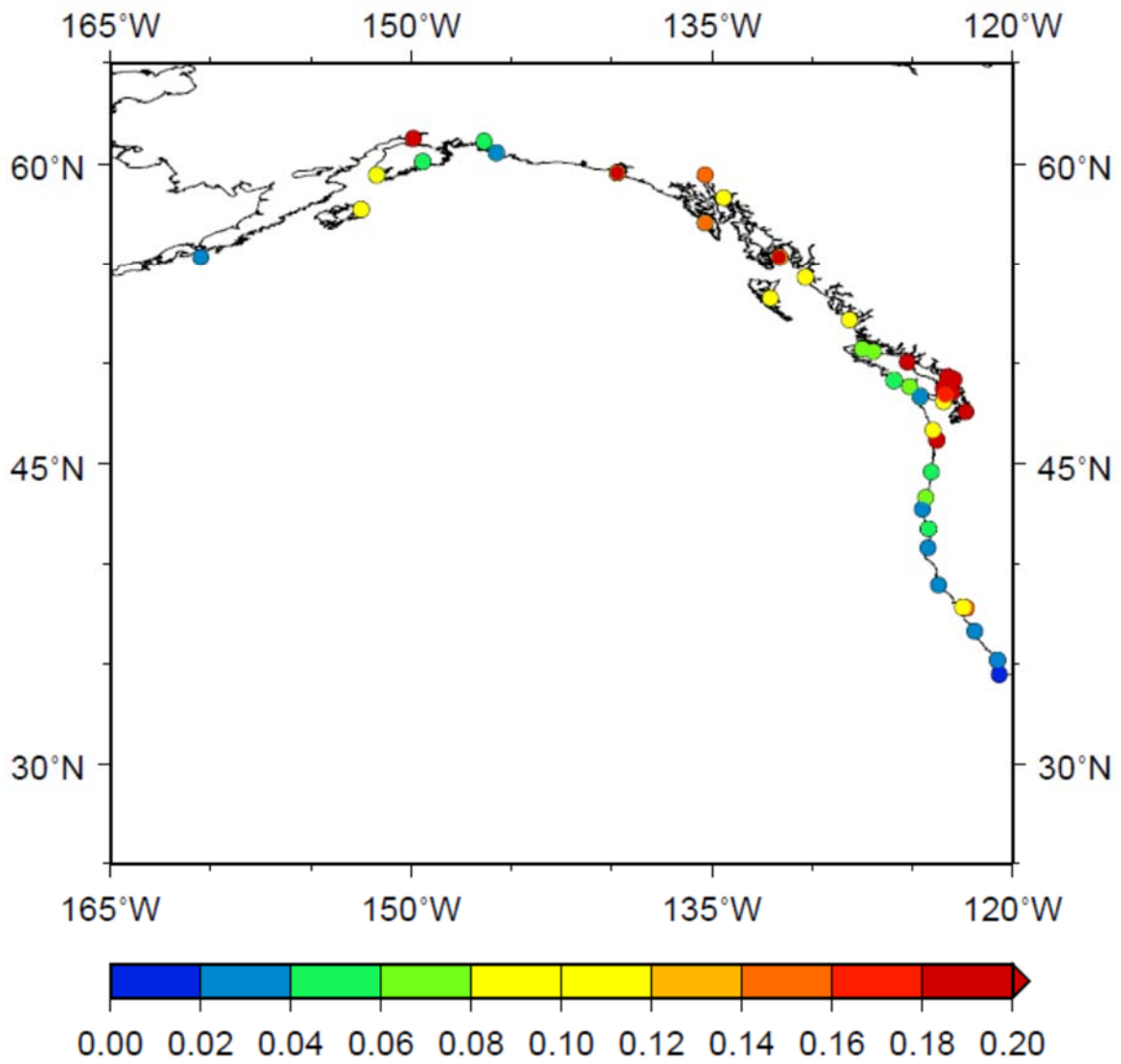




(c)

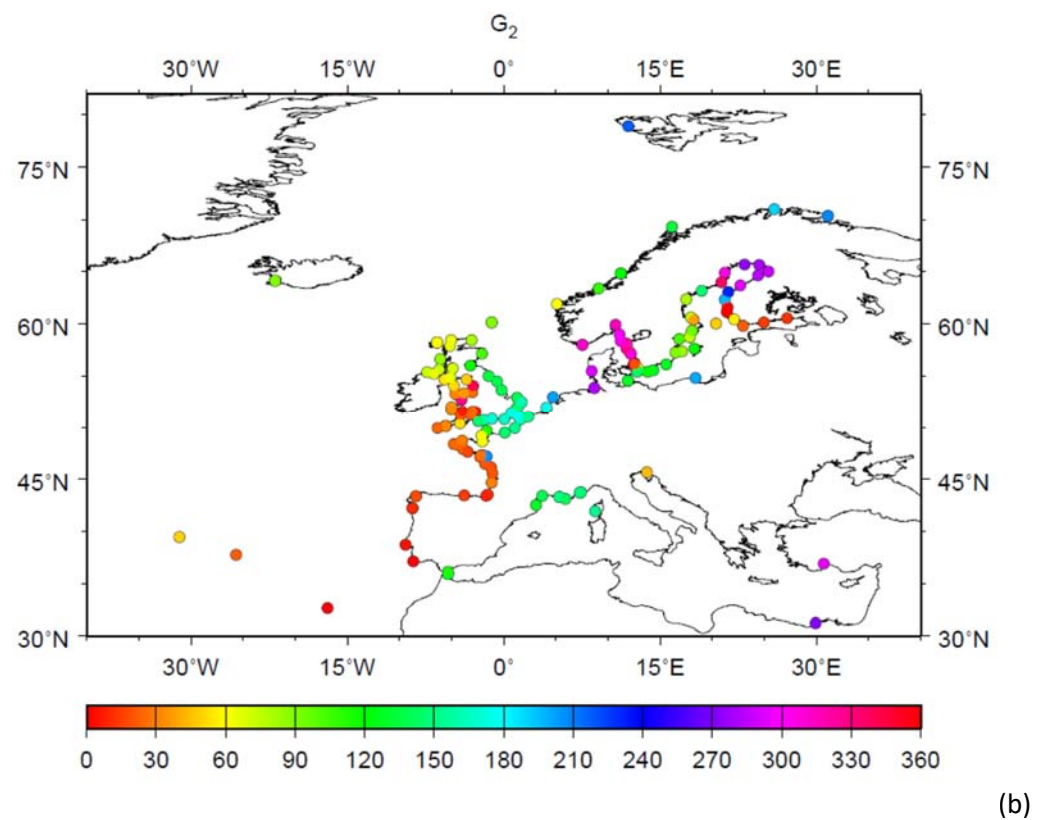
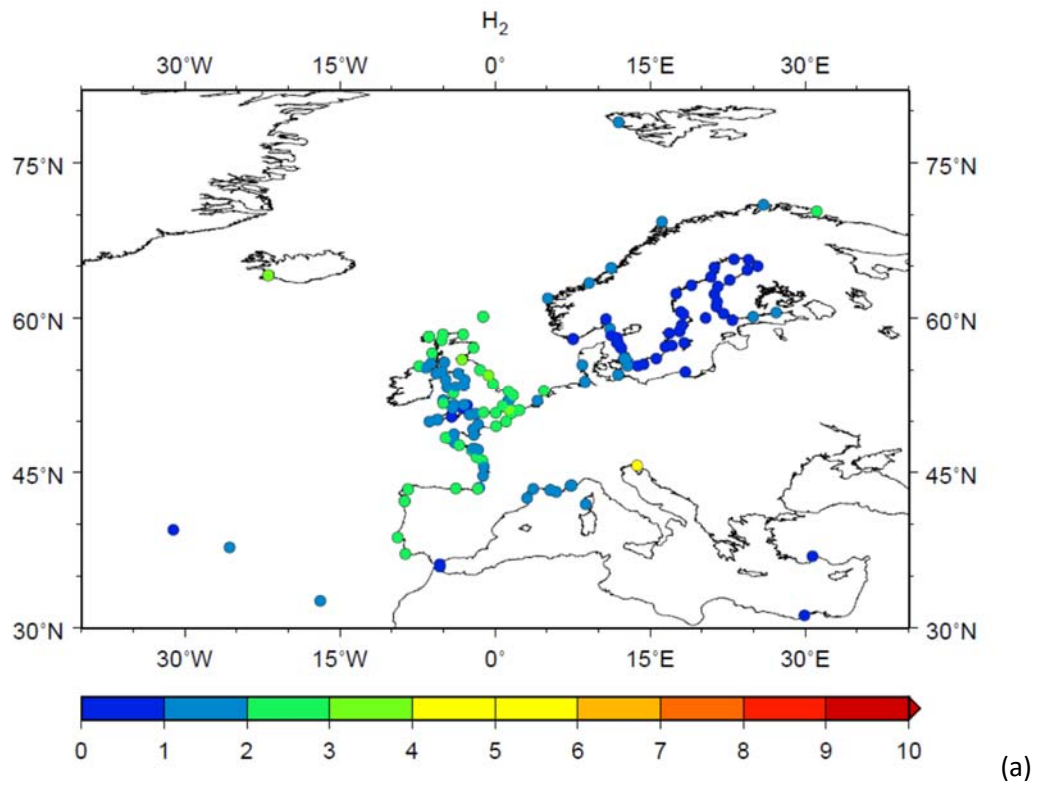


(d)

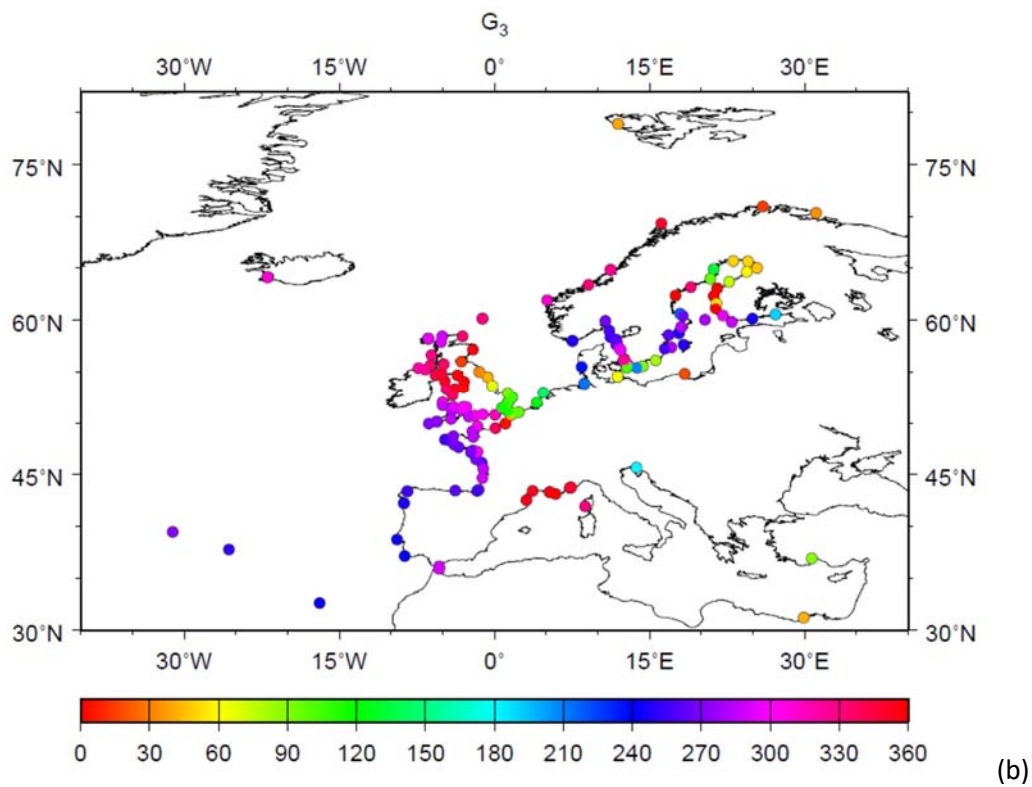
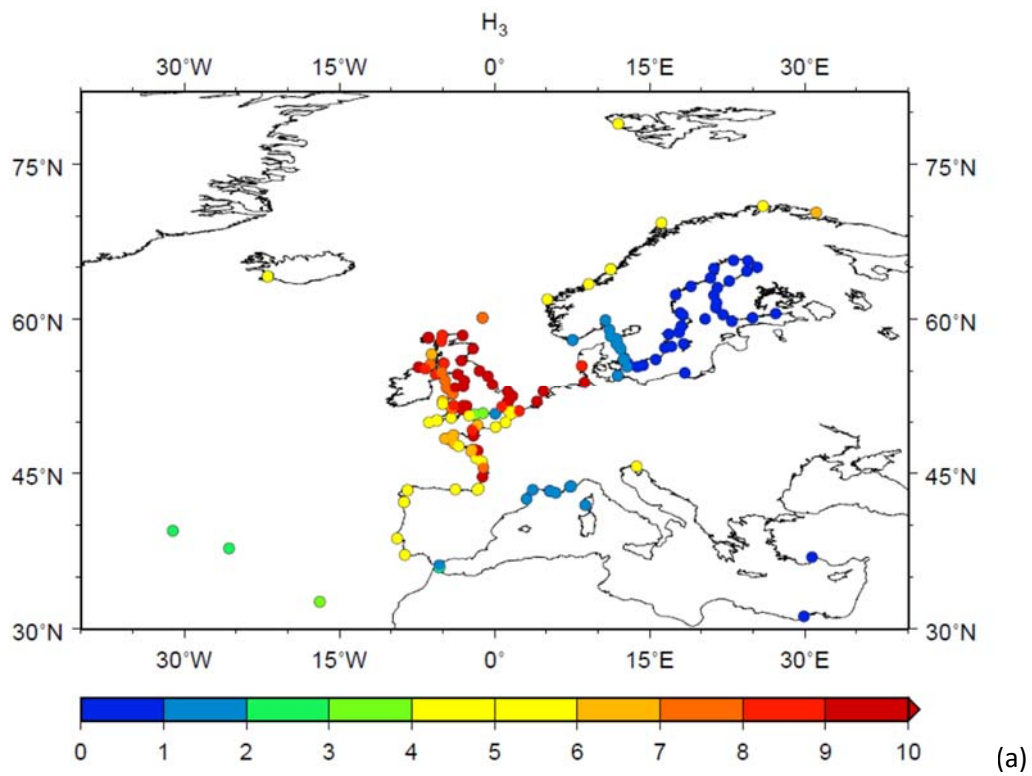


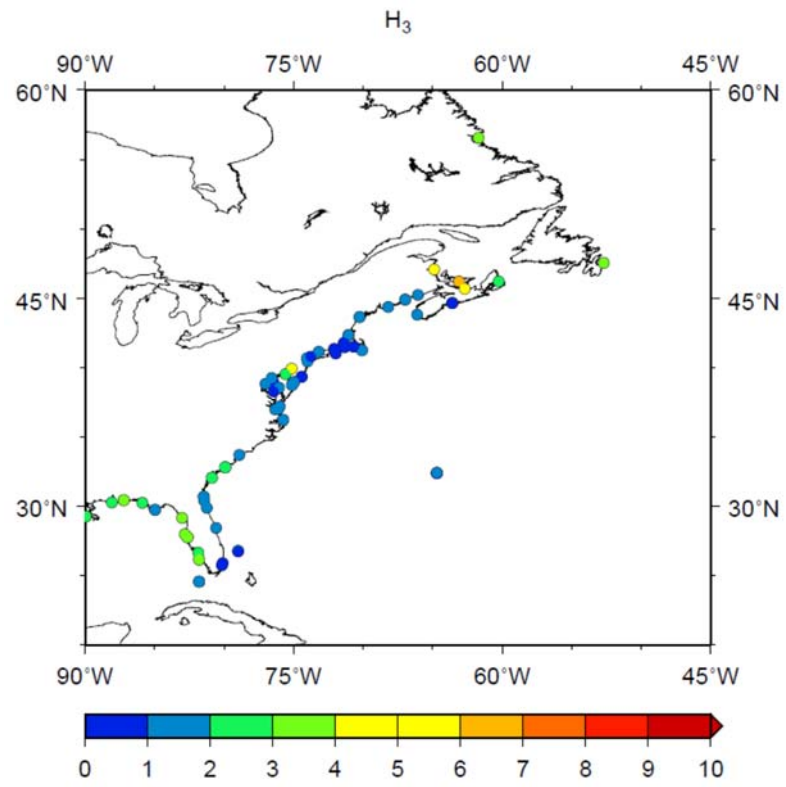
(e)

Supplementary Figure 3. (a) Histogram of variance  $V$  (cm²) for all the records in the analysis, bins of 0.01 cm². Maps of  $V$  in the same units for (b) worldwide, (c) NW Europe, (d) NE America and (e) NW America.

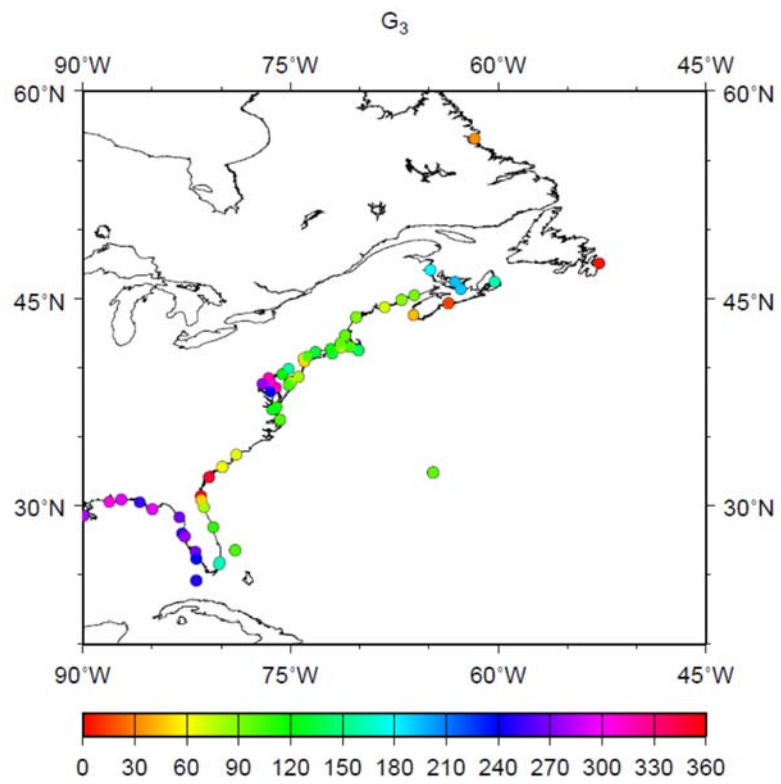


Supplementary Figure 4. (a) Amplitude and (b) Greenwich phase lag of  $M1'$  as in Figure 5(a,b) focusing on NW Europe.



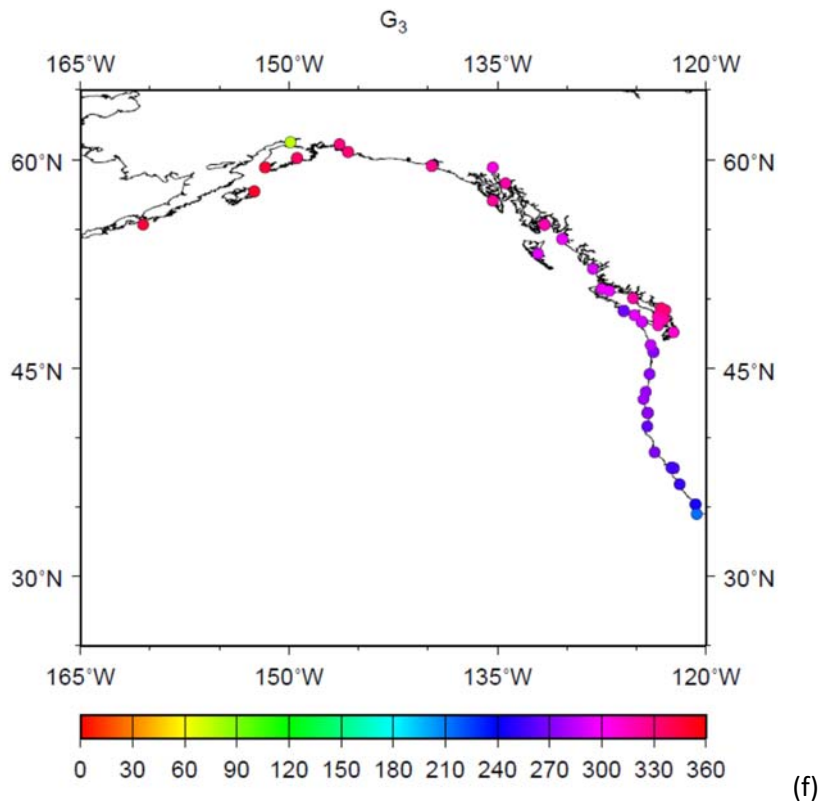
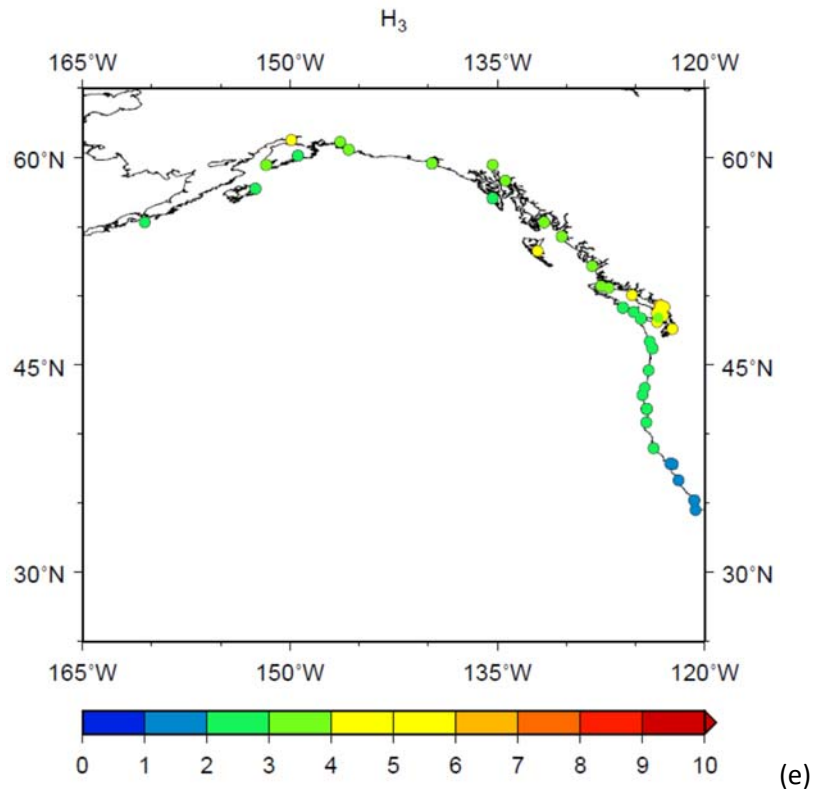


(c)



(d)





Supplementary Figure 5. (a) Amplitude and (b) Greenwich phase lag of M1 as in Figure 7(a,b) focusing on NW Europe; (c) and (d) on the east coast of North America; and (e) and (f) on the west coast of North America.